Rock and Soil Mechanics

Volume 43 | Issue 4 Article 1

6-9-2022

Analysis of preferential flow migration in unsaturated transparent soil

Yun QUE
College of Civil Engineering, Fuzhou University, Fuzhou, Fujian 350116, China

Bin WENG
College of Civil Engineering, Fuzhou University, Fuzhou, Fujian 350116, China

Song-lin CAI
College of Civil Engineering, Fuzhou University, Fuzhou, Fujian 350116, China

Jin-yuan LIU
Department of Civil Engineering, Ryerson University, Toronto, Canada

Custom Citation

QUE Yun, WENG Bin, CAI Song-lin, LIU Jin-yuan, . Analysis of preferential flow migration in unsaturated transparent soil[J]. Rock and Soil Mechanics, 2022, 43(4): 857-867.

Rock and Soil Mechanics 2022 43(4): 857−867 ISSN 1000−7598
https: //doi.org/10.16285/j.rsm.2021.6087 rocksoilmech.researchcommons.org/journal

Analysis of preferential flow migration in unsaturated transparent soil

QUE Yun[1], WENG Bin[1], CAI Song-lin[1], LIU Jin-yuan[2]

1. College of Civil Engineering, Fuzhou University, Fuzhou, Fujian 350116, China
2. Department of Civil Engineering, Ryerson University, Toronto, Canada

Abstract: In order to realize the visualization of unsaturated preferential flow migration of soil, a column device was designed to carry out unsaturated seepage tests. The transparent soil and digital image processing technology were used to establish the relationship between the normalized pixel intensity and the saturation of transparent soil. On this basis, the effects of the connectivity of the preferential flow path and the rotation angle of the adjacent preferential flow path on the preferential flow migration in unsaturated soils were studied by conducting laboratory model tests. The results showed that it was feasible to characterize the saturation of unsaturated transparent soils based on the intensity of image grayscale pixels. The profile of fully connection preferential flow (O-O type) and upper connection preferential flow (O-C type) presented a T-shape. The saturation of the central axis profile was obviously different from that of the central edge profile. In the lower connection preferential flow path (C-O type), the soil oil pressure and matrix potential could not make the fluid enter the preferential flow path to form the preferential flow, in which the trend of infiltration was consistent with the uniform flow. The stable infiltration rate and the wetting front moving velocity of O-C preferential flow were 1.5 times and 1.4 times of those of the C-O type, respectively. A new preferential flow was formed in the area between adjacent O-C preferential flows. The soil in that area reached higher saturation and the growth rate of saturation decreased with the increase of rotation angle. When the preferential flow rotation angle was 90°, 60° and 30°, the stable infiltration rate was respectively 1.5 times, 1.3 times and 1.2 times that of the uniform flow. As the fluid was affected by gravity, the preferential flow with a small rotation angle only infiltrated horizontally along one side of the path. However, the moving velocity of the wetting front was 1.3 times, 1.4 times, and 1.5 times that of uniform flow, respectively. The interaction between adjacent preferential flows was weakened, so it was difficult to form the new preferential flow.

Keywords: transparent soil; normalized pixel intensity; saturation; unsaturated preferential flow; wetting front

1 Introduction

With the modernization and the gradual improvement of ecological protection awareness, the monitoring of soil ecological environment has entered a new research stage. Many new phenomena of water and solute migration in heterogeneous soils have been found, which could not be explained by the traditional unsaturated homogeneous flow. In the existing studies, it has been confirmed that although the content of polluting solute does not exceed the self-cleaning capacity of soil, it will also pollute groundwater and deep soil, and some solutes with low mobility, short degradation cycle and low residue can still be detected within the groundwater level[1−3]. Therefore, there should be a mechanism of flooding and solute moving rapidly to the deep soil, which is the preferential flow.

Preferential flow refers to the phenomenon that the water and solutes in the soil bypass a majority of homogeneous layer matrixes and preferentially reach the infiltration path with good hydraulic conductivity to rapidly migrate to the deeper soil layers and underground water level[4]. As early as the end of the 20th century, 17 scientists at the Monte Verita symposium reached a consensus that preferential flow is widespread and of great research value[5]. According to the difference in the scale of analysis and infiltration mechanism, the preferential flow can be divided into two main categories: macropore flow at the mesoscopic scale and unstable flow at the soil scale[6]. Due to unstable flow, the complex structure in the soil causes water to bypass most of the soil matrix and infiltrate along the preferential flow path, thus giving rise to finger flow and funnel flow depending on their formation mechanisms and flow patterns, as shown in Fig. 1.

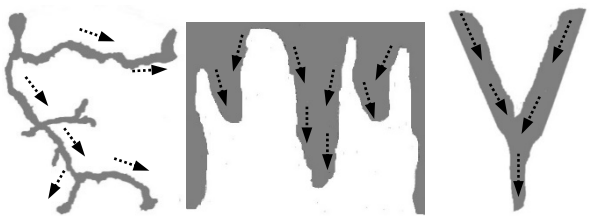

(a) Macropore flow (b) Finger flow (c) Funnel flow

Fig. 1 Profile diagrams of various preferential flows

Received: 17 July 2021 Revised: 17 September 2021
This work was supported by the National Natural Science Foundation of China (No. 41772297).
First author: QUE Yun, male, born in 1980, PhD, Professor, mainly engaged in the teaching and research of slope stability and treatment. E-mail: queyun_2001@fzu.edu.cn

At present, the dyeing tracer method is widely used in the observation of unsaturated preferential flow. Morris et al.[7] studied the physical morphological characteristics and generation mechanism of preferential flow by using bright blue dye and image analysis technology, while comparing TDR observation profiles and penetration curves. Li et al.[8] carried out a comparative analysis of uniform flow and preferential flow tests on no-till soil and plowed soil in autumn in combination with the dyeing tracer method and double-loop method. Wang et al.[9] excavated several longitudinal sections of soils at multiple locations and used bright blue and starch−potassium iodide dyes to trace the preferential flow of soils, respectively. In addition to the dyes mentioned above, some researchers have also employed non-absorbent inorganic ions and radioactive isotopes to do the tracer analysis, and good observation results have been achieved[10−11].

The above research results have improved the knowledge of preferential flow migration patterns in unsaturated soils. However, the internal structure of natural soils is not visible, it is difficult to observe the fluid movement inside the pore directly from the outside. There is no tool to measure the characteristics of water infiltration in pores, so it is difficult to obtain real-time dynamic information in the process of rainfall infiltration. The dyeing tracer method might disturb the preferential flow path during the soil sampling, and part of the dyeing agent can be absorbed by the soil matrix, which directly affects the migration of water and solutes. Therefore, it is urgent to develop a research method to visualize the infiltration process.

Transparent soil is a kind of similar material that has been gradually applied for non-contact observation research in model tests in recent years, and it can effectively solve the bottleneck encountered in observation. The synthetic transparent soil is composed of transparent aggregate and pore fluid, both of which have the same refractive index. In 1990, Mannheimer et al.[12] formulated a transparent mud that approximated a non-Newtonian body, and studied the consolidated transparent mud samples from the physical and mechanical properties to verify the similarity between the transparent material and the actual soil, which laid a foundation for the subsequent development of transparent soils with more stable properties. Currently, the commonly used aggregates for transparent soils are amorphous silica powder with the characteristics similar to clay in geotechnical engineering[13], fused silica sand similar to sandy soil in geotechnical engineering[14−17], and Aquabeads, which is a highly absorbent polymer[18]. In terms of simulating seepage fields, saturated transparent soil was usually used to study the transport of natural soil solutes in early studies. Liu[19] obtained the penetration curve of dyes in the soil with the help of transparent soil. Tabe et al. [20−21] used Aquabeads saturated transparent soil to analyze the two-dimensional seepage and the solute transport in the deep soil, revealing the scouring performance of surfactants for a variety of fluids. Kashuk et al.[22] used transparent soil to analyze the concentration distribution in the process of pollutant transport. Serrano et al.[23] began to use unsaturated transparent soil to simulate Miga sand to realize the transport process of polluting solute in soil under different degrees of saturation. Peters[24] studied the phenomenon of unsaturated uniform flow in soil with the help of quartz sand transparent soil. Liu et al.[25] summarized the research progress based on the permeability characteristics of transparent soil in recent years, and pointed out that the test technology of transparent soil can not only analyze the solute migration and distribution but also has advantages in solving the seepage field and seepage deformation. From the above, it is clear that the simulation of seepage field is mostly concentrated in the field of saturated transparent soil, and there are few studies on non-uniform infiltration of unsaturated transparent soil. In fact, the following problems exist in the current studies on the seepage of unsaturated transparent soil: (1) unsaturated transparent soil has no transparency effect, so it is difficult to visualize water migration in unsaturated transparent soil, and (2) image recognition software such as PIV (particle image velocimetry) technology is not easy to identify and analyze unsaturated transparent soil, making the study of unsaturated transparent soil more difficult.

In view of this, based on the concept of pixel intensity, this paper establishes the relationship between the normalized pixel intensity and the saturation of unsaturated transparent soil. On this basis, the effects of preferential flow paths with different connectivity and the rotation angle of adjacent preferential flow paths on the infiltration of unsaturated soil are analyzed.

2 Relationship between normalized pixel intensity and saturation

2.1 Transparent material properties

Compared with silica gel, fused silica sand does not have large number of microscopic pores inside; compared with glass sand, it has very few impurities, higher purity and better transparency. Therefore, the homogeneous sand with particle sizes between 0.5 mm and 1 mm produced by Donghai Rich Color Mineral Co., Ltd. was used as the research material for unsaturated infiltration tests, and its refractive index is 1.459.

Combining with previous adaptation experience, the mixture of n-tridecane and #15 white oil (mass ratio 1:4) was selected as the pore fluid in this study to simulate the infiltration process of rainfall and realize the visualization study of internal water migration. It was tested that the refractive index of the mixture was also 1.459 at this ratio, which ensured the good transparency of the transparent sandy soil. Fig. 2 shows the effect diagram of transparent soil with different mass ratios of the mixture.

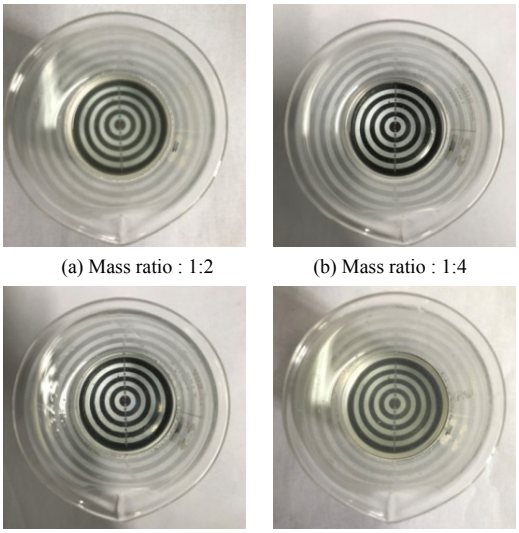

Fig. 2 Effect diagram of transparent soil with different mixture mass ratios

2.2 Testing equipment

Unsaturated seepage was studied using a 500 mm long square column device, as shown in Fig. 3. The internal cross-sectional dimensions of the column were 70 mm×50 mm (length×width). The front and side were made of 7 mm and 10 mm acrylic plexiglass, respectively, with good light transmission. A high-speed digital camera was used to capture high-resolution images with an accuracy of 18 million pixels. The camera was attached to a tripod at a constant distance from the column. The column was placed on the test platform, and the relative position of the camera and the column was adjusted to enable the camera to obtain a complete section of transparent soil. The final distance between the shooting plane and the column observation plane was kept at 400 mm. When the transparent soil was saturated, the black cardboard was used on the back of the column to produce a consistent dark background color, which had a high contrast to the white appearance of the dry transparent soil.

2.3 Testing methods and analysis

The relationship between normalized pixel intensity and degree of saturation was established through the following three steps: (1) definition of normalized pixel intensity; (2) pixel intensity analysis of black and white reference points and transparent soil with different saturation states; (3) fitting relationship between normalized pixel intensity and degree of saturation.

2.3.1 Definition of normalized pixel intensity

Peters et al.[26] studied the relationship between grayscale pixel intensity and degree of saturation in the permeability tests by taking advantage of the gradual change of the color of the transparent soil profile along the column height. The degree of saturation measured by different grayscale pixel intensities was used to record the real-time change during the permeability tests.

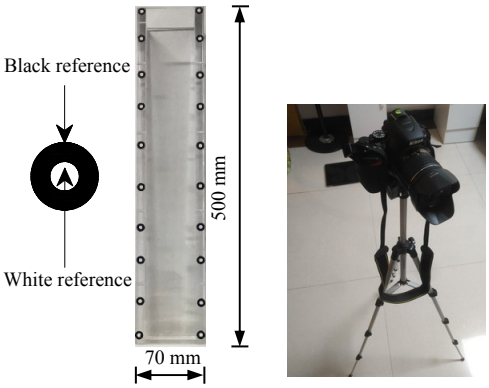

Fig. 3 Device for column tests

In order to determine the degree of saturation of the transparent soil by the variation of column color and verify the linear relationship between the pixel intensity of digital image and the degree of saturation, it is necessary to define the normalized pixel intensity values for each height. The intensity changes between the two limit saturation can be quantified by normalizing pixel intensity $I_N(h)$, which is expressed as

$$I_N(h) = \frac{I(h) - I_{Sr}(h)}{I_{Dr}(h) - I_{Sr}(h)} \quad (1)$$

where h represents the height from the column bottom; $I_{Dr}(h)$ represents the measured value of grayscale pixel intensity of dry soil at a certain height; $I_{Sr}(h)$ represents the measured value of grayscale pixel intensity of saturated soil at a certain height; and $I(h)$ represents the measured grayscale pixel intensity of unsaturated soil at a certain height.

2.3.2 Pixel intensity analysis of transparent soil with different saturation states

The pixel intensities of the black and white reference points distributed at different heights on the column surface was measured. Since the color of the reference points did not change, the pixel intensity of black and white reference points could be used to correct for changes in pixel intensity of the profile due to changes

in the saturation of transparent soil. Fig. 4 shows the typical changes of the black and white reference colors along the column height and the grayscale pixel intensity of transparent soil with different saturation states. It can be seen from the figure that:

(1) Even though each reference point was made of the same material, both the black and white reference areas had a higher pixel intensity at the top of the column than at the bottom, because the light source on the column surface was mainly provided by the laboratory overhead lamp. Compared to reference points at the bottom, the black reference point at the top had an increase of about 23 pixel intensities, while the white reference point at the top had an increase of about 34 pixel intensities. At the same time, due to the limitations of the camera parameter settings and the slight deviation of the lens angle, the intensity of black and white pixels in the captured image could not reach the full state. As a result, the pixel intensity could not reach exactly 0 and 255, but the overall pixel intensity showed a monotonic increasing trend along the column height.

(2) The profile color of transparent soil could not reach pure white or black under the two extreme critical conditions of the degree of saturation of 0 or 1. In order to verify the color changes of transparent soil under the two limit degrees of saturation, the columns were filled with fully saturated transparent soil and fully dried fused silica sand respectively, and the images of the column profiles of these two groups were collected. When the saturation S_r =1, it can be observed that the black background had a higher degree of transmission on the transparent soil profile, but it was slightly lower than the pixel intensity of the black reference point. When the saturation S_r=0, in the completely dry soil column, the black background cannot be transmitted and appeared bright white, but it was slightly less than the pixel intensity of the white reference point. It can be seen that regardless of whether the transparent soil was completely saturated or completely dry, the variation trend of pixel intensity along the column height was basically consistent with the black and white reference points. The pixel intensity of the critical saturation of transparent soil fluctuated from left to right due to the color difference of the image caused by the uneven local distribution of soil particles.

(3) When the degree of saturation was $0<S_r<1$, that is, the pore fluid infiltrated freely at the top of the column, the grayscale pixel intensity of the transparent soil profile along the column height was between those of the saturated soil and dry soil, reaching a semi-saturated state. In the range of 150 mm height along the bottom of the column, the transparent soil was close to saturation, and the changing trend of pixel intensity was similar to that of fully saturated transparent soil. When the height range exceeded 150 mm, the transparent soil began to change from the saturated state to the unsaturated state, resulting in a sudden change in pixel intensity and an air peak. This pixel intensity gradually approached the pixel intensity of dry soil, presenting an increasing trend of fluctuation. This region of sudden change is called the gas−liquid boundary zone.

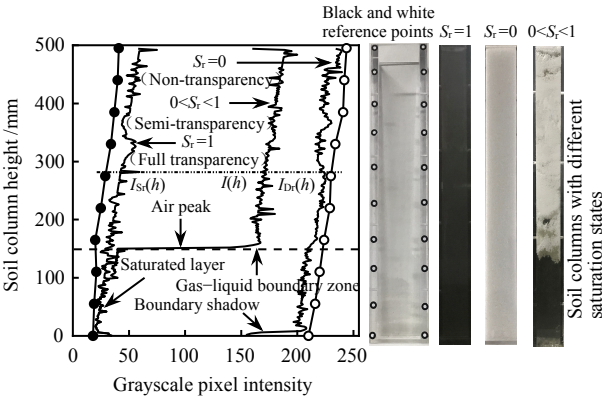

Fig. 4 Variation in pixel intensity of the black and white reference points with different height distribution and the soil column with different saturation

2.3.3 Fitting relationship between normalized pixel intensity and degree of saturation

The limit value of normalized pixel intensity is correlated with the limit value of soil degree of saturation. With the variation of soil degree of saturation, the normalized pixel intensity also shows dynamic changes, while this corresponding relationship is still uncertain. If such a functional relationship can be measured experimentally, the normalized pixel intensity can be back-calculated by detecting the grayscale pixel intensity of any transparent soil profile. Thus, the degree of saturation of transparent soil in the region of interest can be deduced from the corresponding functional relationship.

Synthetic transparent soil with different degrees of saturation were prepared and divided into six saturation gradients (namely, 0.0, 0.2, 0.4, 0.6, 0.8, 1.0). By testing the average pixel intensity of the selected regions of transparent soil samples with different degrees of saturation, the corresponding values of average pixel intensity at different degrees of saturation were obtained, as shown in Table 1. As can be seen from the table, the degree of saturation and average pixel intensity were not in complete linear correspondence, and the regularity between them could not be obtained. For this reason, the piecewise linear function relationship was fitted by collecting a large number of profiled pixel points to reveal the normalized pixel intensities of transparent

soil under different degrees of saturation. Fig. 5 shows the fitted relationship between the degree of saturation and normalized pixel intensity. Four parts of the column profile image collected during the uniform infiltration of unsaturated soil were intercepted, and the color change of transparent soil from the dry state to the saturated state is indicated by ①,②, ③ and ④, respectively, which were located on the four positions of the fitted line segment.

As can be seen from the figure, the intensity of grayscale pixel showed an overall decreasing trend with the increase of degree of saturation, which could be divided into three fitted lines with good linear fitting. Therefore, it is feasible to characterize the non-uniform seepage process of unsaturated transparent soil by the three-stage fitting linear function of saturation and normalized pixel intensity. For the transparent soil with unknown saturation, the grayscale pixel intensity is tested, and then the average value can be obtained. The normalized pixel intensity value is obtained from Eq. (1), and then the required saturation of transparent soil can be obtained by using the three-stage fitting linear function in Fig. 5.

Table 1 Corresponding values of average pixel intensity at different degrees of saturation

Degree of saturation S_r	0.0	0.2	0.4	0.6	0.8	1.0
Average pixel intensity I	222	214	198	189	120	23
Normalized pixel intensity I_N	1.000	0.962	0.880	0.838	0.492	0.000

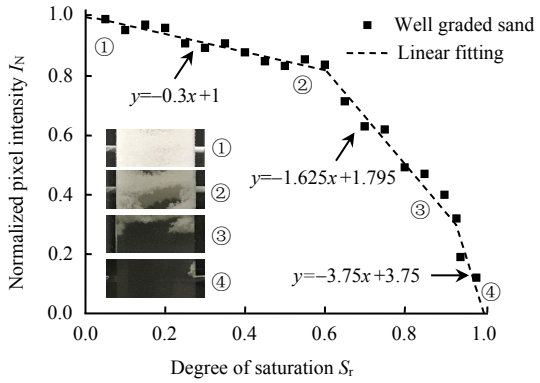

Fig. 5 Fitting relationship between degree of saturation and normalized pixel intensity

3 Design of test models for different preferential flow paths

3.1 Preferential flow path model with different connectivity

The effect of the connectivity of the preferential flow path on the preferential flow infiltration was investigated using a soil column with an artificial preferential flow path. The wall thickness of the acrylic column was 5 mm, and its internal size was 20 cm×2 cm×450 cm. Since the width of the column was relatively thin, the column could be regarded as a two-dimensional oil infiltration system. The artificial preferential flow path was replaced by a rigid PC round tube with a diameter of 8 mm, which had high transparency. At the same time, a micro electric drill was used to drill the uniformly densely distributed fine holes on the tube wall to ensure the smooth oil exchange with surrounding soil in the path, as shown in Fig. 6.

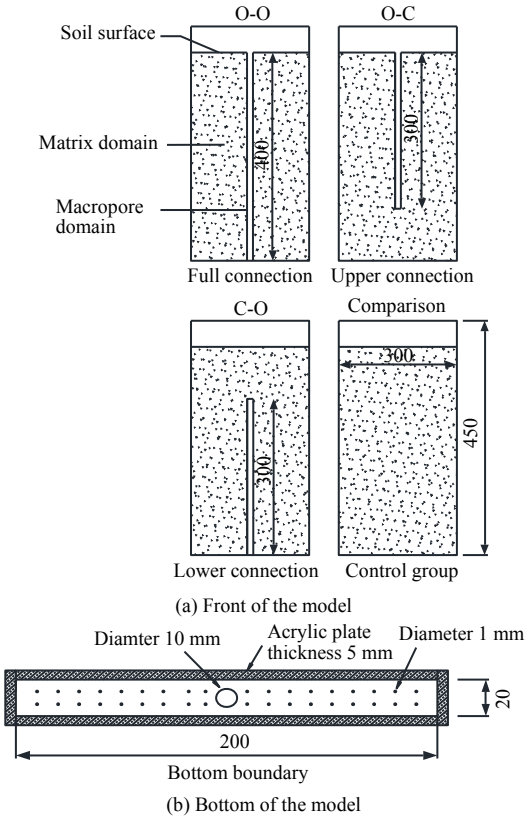

Fig. 6 Schematic diagram of preferential flow path connectivity tests (unit: mm)

Figure 6 shows the schematic diagram of the preferential flow path connectivity test model. As shown in the figure, the types of the artificial preferential flow path were set as follows: full connection (the path was exposed on the soil surface, and the outlet was at the bottom of the soil, O-O type); upper connection (the path was exposed on the soil surface, and the outlet was inside the soil, O-C type); lower connection (the path opening was buried inside the soil, and the outlet is at the bottom of the column, C-O type) and the control group (without the preferential flow path), where O represented Open and C represented Closed. The length of the full connection preferential flow path was 40 cm, and the length of the upper connection and lower connection paths were 30 cm. The artificial preferential flow path was installed in the middle of the soil column before filling with sand to ensure the compaction between the soil and the path.

And a control model without the preferential flow path was set up, and each group of tests was repeated three times.

The water head was kept constant by using a Mahalanobis bottle, and the water head (the height difference between the boundary oil surface and the soil surface of the test device) was 30 mm. After the mixture began to enter the column, the volume of infiltration solution and the depth of the wetting front were recorded until the infiltration of the wetting front was completed. Holes with a diameter of 1 mm were evenly distributed at the bottom of the column, which could be used as outlet holes in the matrix domain and also to maintain stable air pressure in the column. Before loading sand, a filter screen was laid at the bottom of the column to prevent some particles from leaking out through the small holes and ensure smooth exhaust during the infiltration of the mixture. The hole with a diameter of 10 mm in the middle was used as the outlet hole of the preferential domain, and the lower end was connected with a hose. In the process of seepage, the effluent was distributed along its own path. Two 100 mL volumetric flasks were used to take up the effluent from the two domains, and the effluent volume and time were measured.

3.2 Model of adjacent preferential flow path with different rotation angles

A large number of indoor and field tests have shown that there may be adjacent macropores/microcracks with different connectivity and sizes in a unit volume of soil. These preferential flow paths construct various connectivity networks inside the soil, which have varying degrees of influence on the infiltration, migration, adsorption, and distribution of water and solutes in the soil. As shown in Fig. 7, in order to analyze the influence of adjacent preferential flow path on the infiltration process, the length, thickness, height and loading height of the selected transparent column were 30 cm, 1 cm, 24 cm, and 20 cm, respectively. Two preferential flow paths were set in the soil column, both of which belonged to the upper connection with a length of 10 cm and a spacing of 14 cm. One of the preferential flow paths was vertical, and the other path was set along the vertical clockwise with three different rotation angles of 30°, 60°, and 90°. A Mahalanobis bottle with an inner diameter of 8 cm and a height of 60 cm was used to provide the input solution, and the water head was controlled at about 30 mm. At the bottom of the column, an outlet hole with a diameter of 1 mm was evenly distributed. The mixed oil was discharged from the outlet hole and finally collected in the volumetric flask.

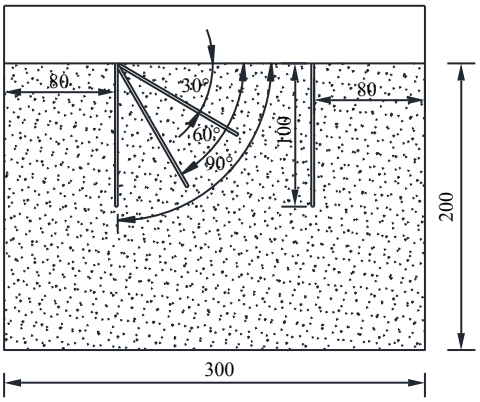

Fig. 7 Diagram of adjacent preferential flow path test device (unit: mm)

4 Results

4.1 Influence of the connectivity of preferential flow path

4.1.1 Influence of the preferential flow path connectivity on the process of wetting front movement

Figure 8 shows the patterns of wetting fronts in different connectivity preferential flow path profiles with time. The test simulated the infiltration of accumulated oil in the dry soil. There was an obvious potential gradient for oil between the wetting front and the dry soil in front of the wetting front, which accelerated the downward movement of the wetting front. It can be seen from the figure that with the increase of oil content in transparent soil, the oil potential gradient inside and outside the membrane gradually decreased, and the advancing rate of the wetting front also gradually slowed down. The O-O type preferential flow path was connected with the soil surface. Under the condition of constant oil supply, a small part of the fluid in the preferential flow path migrated in the soil matrix, while most of the fluid quickly reached the bottom of the path and infiltrated horizontally along the small holes in the preferential flow path. The infiltration profile presented a black trajectory, and the overall performance was T-shaped. The upper flow path gradually infiltrated to the center of the preferential flow path along the soil matrix and had an apparent preferential flow path. The fluid in the O-C type preferential flow path entered the soil in two parts: horizontal infiltration along the side wall of the path and vertical infiltration along the matrix micropores at the bottom of the path. For the upper connection type of preferential flow path, the horizontal diffusion radius was larger and had a relatively smooth diffusion arc, while its longitudinal penetration was significantly different from the longitudinal infiltration trajectory of the full connection type of preferential flow path. The C-O type preferential flow path with unconnected

surfaces had no effect on the advancing process of the wetting front, and the migration of the wetting front was not significantly different from that of the control group. This is mainly because the oil supply of soil in the front of the wetting front was supplied by the oil discharge from the upper wet soil layer, and the infiltration rate of the upper layer determined the infiltration rate of the lower layer to a certain extent. Therefore, the pressure with a smaller oil potential gradient would hinder the preferential inflow and infiltration, leading to the preferential flow path at the lower end of the soil being difficult to play a role.

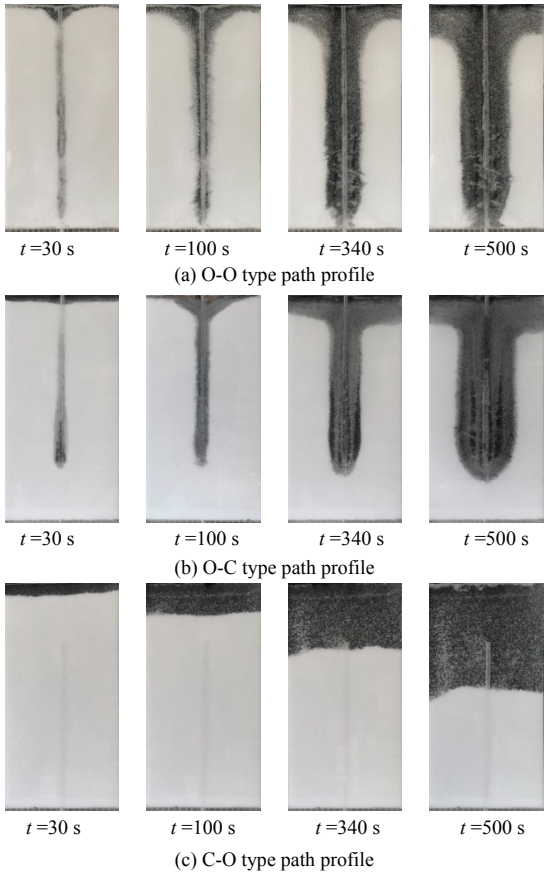

Fig. 8 Migration patterns of the wetting front in the profile of preferential flow paths with different connectivity

4.1.2 Influence of the preferential flow path connectivity on the degree of saturation distribution of transparent soil profile

To analyze the variation of degree of saturation of infiltration profile along the height of soil column at a specific moment for preferential flow paths with different connectivity, the original infiltration images of soil column at three specific times (100, 340, 500 s) were selected for the degree of saturation analysis. Due to the non-uniformity of preferential flow infiltration, different preferential flow paths were formed within transparent sand, which made the research more difficult. Therefore, with the help of digital image processing technology, image processing was carried out on the infiltration path. First, the interference boundary area was eliminated, then the required preferential flow profile was extracted, and finally, it was matched with the degree of saturation. Taking the analysis of O-O type preferential flow path at 340 s as an example, Fig. 9 shows the image processing of a preferential flow profile. According to the figure, the original sequence images were binarized to eliminate background interference. Some noise points in the binarization images were denoised by median filtering to obtain higher-quality images. Finally, the edge recognition of the study area was carried out to improve the analysis effect. The extracted infiltration profile was a continuous line segment, which was actually a grayscale value set of discrete pixels.

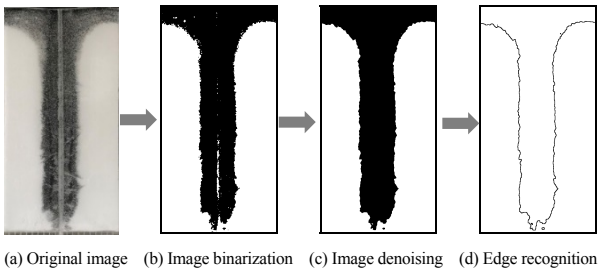

Fig. 9 Image processing method of the extracted contour of O-O type preferential flow

Since the structure of the infiltration profile of preferential flows with different connectivity at a specific time was basically symmetrical, the infiltration characteristics on both sides were similar. Therefore, the image can be cropped with the central axis of the preferential flow as the boundary, and the left profile was taken for saturation analysis. Two longitudinal sections were set at positions 1 cm and 5 cm away from the central axis, respectively, and the saturation distribution was studied according to the grayscale value change of section I and section II along with the column height.

Figure 10 shows the degree of saturation distribution of transparent soil profile with different connectivity preferential flow paths. It can be seen from the figure that there was a great difference in the degree of saturation distribution of the corresponding section when infiltrating along flow paths with different connectivity. The degree of saturation of section I near the central axis of preferential flow was higher than that of section II near the edge. The difference in the degree of saturation distribution between the two sections of O-O type preferential flow was pronounced. When the infiltration time reached 500 s, the average degree of saturation of section I was about twice that of section II. It can be found that the O-O type preferential flow path had a great impact on the

infiltration characteristics of transparent soil. In addition, the degree of saturation of different sections was basically the same along the column height. With the increase of infiltration time, the degree of saturation increased, which showed a good gradual change of saturation. The difference of saturation distribution between the two sections of O-C type preferential flow was the second. At 500 s, the average degree of saturation of section I was about 30% greater than that of section II. The average degree of saturation of section I and section II along the column height gradually approached, and part of the infiltration trajectory above the O-C type preferential flow port is gradually saturated from the center to both sides. At the same time, it can be found that the O-C type preferential flow had a prominent wetting front at different sections. The wetting front of section I went down with time, while

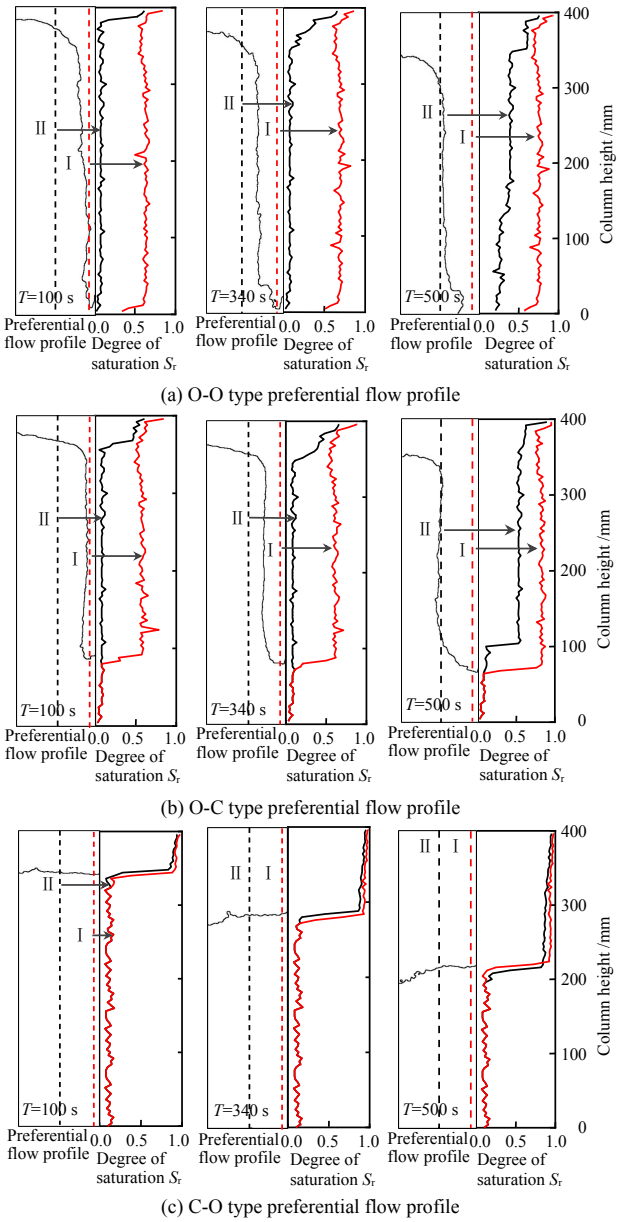

(a) O-O type preferential flow profile

(b) O-C type preferential flow profile

(c) C-O type preferential flow profile

Fig. 10 Saturation distribution of the transparent soil profile of preferential flow paths with different connectivity

the wetting front of section II was basically stable at the upper end of the path in the early stage of infiltration and moved slowly. For the C-O type preferential flow, the degree of saturation distribution of the corresponding section was similar, moving downward along the consistent wetting front. There was no preferential infiltration path, and the oil infiltration was uniform as a whole. Therefore, the path of C-O type preferential flow had little effect on the infiltration process, which was similar to the saturation distribution of the profile without preferential flow path.

4.1.3 Influence of the preferential flow path connectivity on the infiltration process of transparent soil

Through the analysis of the morphological characteristics of fluid infiltration, it is necessary to further quantify the characteristics of preferential flow and determine the difference between preferential flow and uniform infiltration. Therefore, in order to analyze the influence of preferential flow on the infiltration process of transparent soil, the commonly used constant head infiltration method was selected for indoor infiltration tests, and the infiltration capacity of soil was expressed from the variation of infiltration rate and cumulative infiltration volume over time.

Figure 11 shows the variation of the infiltration rate of preferential flow paths with different connectivity in transparent soil with time and the variation of the wetting front movement with time. It can be seen that in the initial stage, most of the fluid in the column of O-O type preferential flow path directly reached the bottom boundary from the surface of the soil column through the path, and the infiltration rate always remained stable. In contrast, the curves of the infiltration rate of O-C type and C-O type preferential flow paths over time were relatively smooth. They firstly decreased rapidly and then tended to be stable with time. However, in the early stage of infiltration, the fluid in the preferential flow path rapidly filled the O-C type path and diffused to the surrounding soil along the path. Therefore, the infiltration rate of the fluid in the O-C type preferential flow path was much higher than that in the C-O type preferential flow path and control group. As the infiltration continued, the soil matrix potential decreased, and the infiltration rate in the soil column with all types of preferential flow paths decreased except the O-O type preferential flow path. Most of the fluids in the O-C type preferential flow path infiltrated horizontally through the side wall of the path and infiltrated vertically through the bottom of the path as the oil supply point. Therefore, the infiltration rate of the O-C type preferential flow path was still about 2 times faster than that in the C-O type preferential flow path and control group. Since the C-O type preferential flow path was deeply buried in the soil, the oil pressure and matrix potential within

the soil were not enough to make the fluid enter the preferential flow path, so it was difficult to form the preferential flow, which had little impact on the infiltration. This is roughly consistent with the variation curve of infiltration rate in the control group.

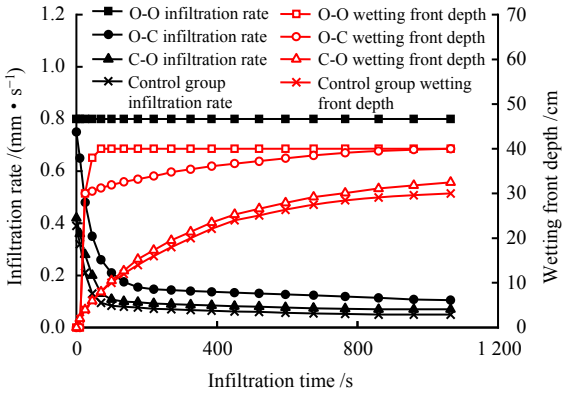

Fig. 11 Variation curves of infiltration rate and wetting front movement with time of different preferential flow paths with different connectivity

It can be seen from Fig. 11 that the wetting front of the O-O type preferential flow path quickly reached the bottom of the soil layer, after which part of the fluid began to infiltrate horizontally along the side wall of the path. For the O-C type preferential flow path, when the fluid reached the bottom matrix layer, the moving process of the wetting front was blocked, and many small holes on the side made most of the fluid infiltrate horizontally along the path and a small part of the fluid gradually diffuse downward. As a result, the changing trend of wetting front in the O-C type preferential flow was faster than that in the C-O preferential flow and control group, and the moving speed was about 1.4 times that of in the C-O type preferential flow and control group. The wetting front of the soil column in the C-O type preferential flow and control group was basically the same. After 1 065 s of infiltration, the wetting front depth was about 30 cm, and the wetting front of the soil column with the O-C type preferential flow had reached the bottom. This is because the C-O type preferential flow path was deeply buried in the soil, forming dead holes, which had little effect on fluid infiltration.

Table 2 shows the comparison of cumulative infiltration volume and stable infiltration rate under different connectivity. The O-C preferential flow path had an important impact on increasing the cum-ulative infiltration. The fluid entering the path could flow into the matrix along different directions, and the infiltration volume was greatly increased. The stable infiltration rate of the O-C type preferential flow was 1.5 times that of the C-O type preferential flow and 2.1 times than that of the control group. The stable infiltration rate of the control group was about 0.30 cm/min, which infiltrated slowly and uniformly, and the cumulative infiltration volume was stable in the upper part of the soil within a given time. Therefore, the existence of large macropores/ microcracks in the soil surface had a significant effect on the cumulative infiltration amount. The existence of large macropores/microcracks in the surface layer of soil increased the pressure potential of soil and improved the moving rate of wetting front, which led to the need for more water in the soil to reach saturation and promoted the growth of cumulative infiltration and stable infiltration to some extent. It can be found that connecting the preferential flow path existing in the soil surface layer could improve its actual water storage capacity and water use efficiency.

Table 2 Comparison of cumulative infiltration and stable infiltration rate of macropores with different connectivity

Pore type	Cumulative infiltration volume /cm				Stable infiltration rate /(cm • min^{-1})
	1.5 min	3 min	6 min	10 min	
O-O type	7.2	14.4	28.8	48	4.80
O-C type	4.1	5.9	8.5	11.7	0.63
C-O type	2.3	3.2	4.9	6.9	0.42
Control group	1.8	2.6	3.8	5.3	0.30

4.2 Influence of the rotation angle of adjacent preferential flow

4.2.1 Influence of the rotation angle of preferential flow path on the wetting front movement

Figure 12 shows the wetting front after the fluid was input into the soil column with different preferential flow path rotation angles. As shown in the figure, at the initial stage of infiltration, the soil column profile with two preferential flow paths can clearly observe the rapid entry path of oil and the formation of preferential flow. There were two wetting fronts in the 30 cm long soil column, presenting different infiltration patterns, and the peak values were higher than those of the control group, indicating that the adjacent preferential flow had a pronounced effect on the surrounding soil. When the rotation angle of two O-C type adjacent preferential flow paths was 90°, the fluid rapidly passed through the paths to reach the deep part of the soil, and then continued to migrate along with the horizontal and vertical directions under the action of matrix potential and gravitational potential. The infiltration characteristics of the two vertical preferential flows were basically the same and gradually showed a wave type. With the decrease of the rotation angle, the infiltration of fluid along the horizontal direction became more obvious. The region between the two preferential flows first reached a high saturation state, which gradually formed a new seepage path, and then

spread continuously from the middle to the surrounding. In contrast, the control group showed parallel infiltration as a whole due to the absence of preferential flow paths. No new preferential flow path was formed, and the infiltration was relatively slow. Therefore, the adjacent preferential flows with different rotation angles would have a great influence on the movement process of the wetting front.

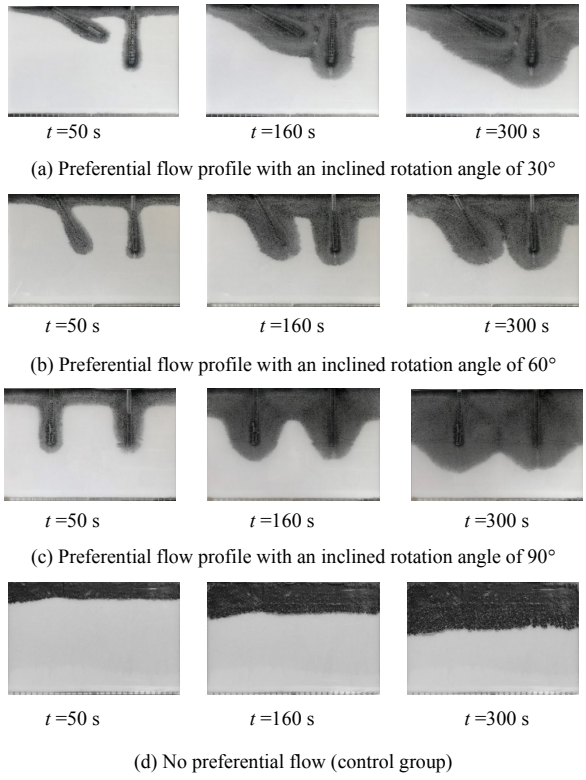

Fig. 12 Migration patterns of the wetting front in the profile of different adjacent inclined preferential flows

4.2.2 Influence of the rotation angle of preferential flow path on the saturation distribution of transparent soil profile

Compared with the symmetry of the infiltration saturation profile of the soil column with a single preferential flow path, the existence of adjacent preferential flows made the infiltration trajectory more complex. Therefore, the use of image recognition technology to extract the preferential flow profile could make the analysis process more intuitive. Fig. 13 shows the sampling position of transparent soil. As shown in the figure, in the soil column with adjacent preferential flows with different rotation angles, three intensity sections of grayscale pixels were selected along the two sides of preferential flow and the symmetrical position of adjacent preferential flow for saturation analysis. Sections I and III on both sides of the preferential flow path were 4 cm away from the soil column boundary, while two grayscale sections were selected for saturation analysis at three equal points for the control group without the presence of preferential flow.

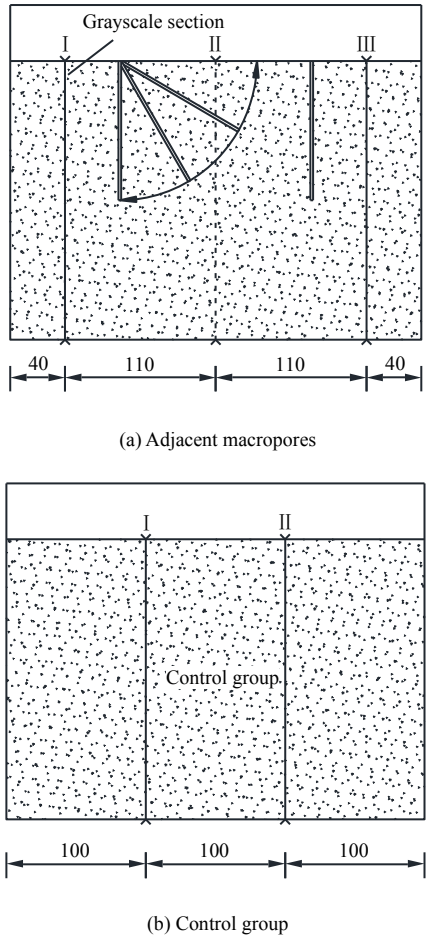

Fig. 13 Schematic diagram of profile location of transparent soils (units: mm)

Figure 14 shows the saturation distribution of transparent soil profiles with adjacent preferential flows at different rotation angles. It can be seen that the contours of the infiltration profiles at different moments on the right side corresponded to the degree of saturation distribution of three different sections along the column height, and the different sections can be distinguished by the color of the line segments. There was a great difference in the degree of saturation distribution of the section corresponding to the infiltration of preferential flow with different rotation angles, and there was a prominent wetting front. The degree of saturation of section II between adjacent preferential flows was higher than that section I and section III on both sides of preferential flows. With the increase of rotation angle, the growth rate of the degree of saturation of section II gradually decreased, and that of section I gradually increased. When the rotation angle was 30°, the growth rate of the degree of saturation of section II along the column height was the fastest, showing an

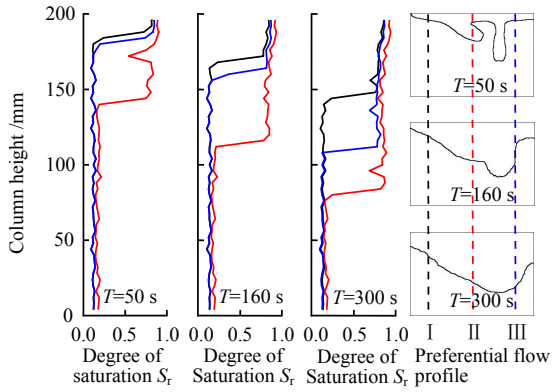

(a) Adjacent preferential flow profile with a rotation angle of 30°

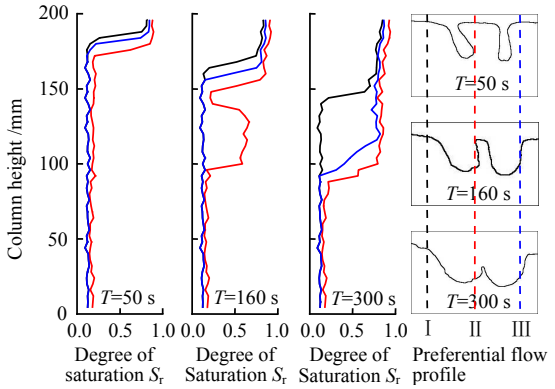

(b) Adjacent preferential flow profile with a rotation angle of 60°

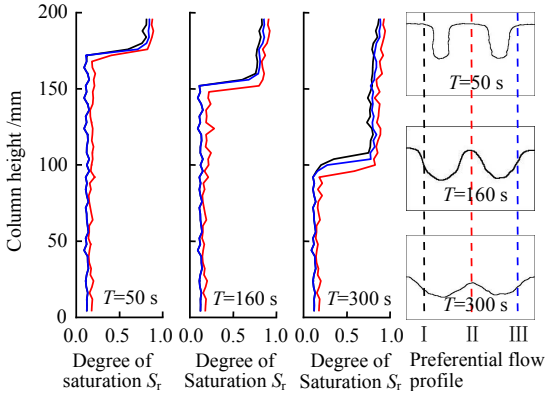

(c) Adjacent preferential flow profile with a rotation angle of 90°

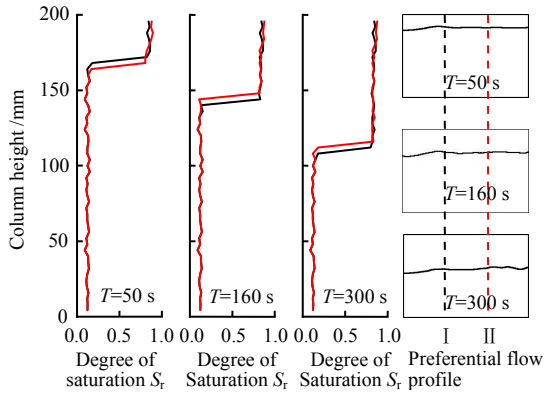

(d) No preferential flow (control group)

Fig. 14 Saturation distribution of adjacent preferential flow transparent soil profiles with different rotation angles

obvious gradient compared to the degree of saturation distribution of other sections, with a visible preferential infiltration path; when the rotation angle was 60°, the growth trend of the degree of saturation of sections II and III was gradually unified with time, but the increase of rotation angle did not effectively change the saturation distribution at section I; when the rotation angle increased to 90°, the infiltration trajectories at each section were highly consistent, and the oil content moved downward along a relatively stable wetting front. The control group also verified that when there was no preferential flow, the variation of the degree of saturation at each section was highly consistent, and the preferential flow did not occur with the change of infiltration time. Therefore, the preferential flow path with different rotation angles had a significant influence on the degree of saturation distribution of the infiltration profile.

4.2.3 Influence of the rotation angle of preferential flow path on the infiltration process of unsaturated transparent soil

Figure 15 shows the variation curves of infiltration rate, cumulative infiltration volume, and wetting front of transparent sand with time. As observed in the figure, at the initial infiltration stage, the infiltration rate was about 0.65 mm/s, which was 1.7 times that of the control group. As the infiltration proceeded, the infiltration rate decreased sharply and then tended to a flat state until stable infiltration. It can also be found that the adjacent preferential infiltration with a rotation angle of 90° was the fastest, and the cumulative infiltration amount was the largest. With the decrease of rotation angle, the infiltration rate and cumulative infiltration volume were also reduced correspondingly. While the control group without the preferential flow path had the slowest infiltration rate, and the cumulative infiltration volume was at a low level. The stable infiltration rate of preferential flow with a rotation angle of 90°, 60°, and 30° was 1.5, 1.3, and 1.2 times that of the control group, respectively. This is because the horizontal infiltration of the fluid along the path became more obvious with the increase of the rotation angle of the adjacent preferential flow, while the fluid in the inclined preferential flow only infiltrated obliquely downward along the small pore on one side of the path due to the action of gravity, with relatively few infiltration paths. It is worth noting that the moving velocity of the wetting front of preferential flow with a rotation angle of 90°, 60°, and 30° was 1.3, 1.4, and 1.5 times that of the control group, respectively. The larger the rotation angle of adjacent preferential flow was, the smaller the depth of the wetting front, which was just opposite to the variation of infiltration rate. This is because when the rotation angle increased, the distance between the two preferential flows also increased, and the interaction between the two was

weakened. In this way, it was difficult to form a more consistent preferential infiltration channel, and the infiltration path of the fluid was more dispersed, which was not conducive to the downward movement of the wetting front.

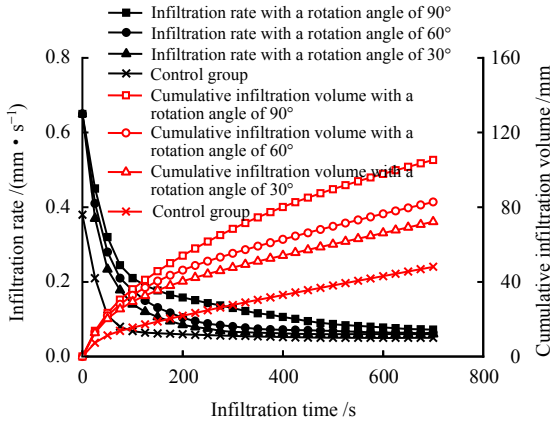

(a) Curves of infiltration rate and cumulative infiltration volume with time

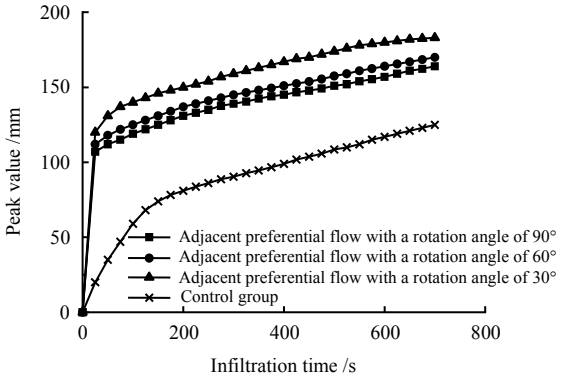

(b) Variation curves of wetting front with time

Fig. 15 Influence of adjacent preferential flow paths on infiltration process

5 Conclusions

(1) The relationship between the normalized pixel intensity and the saturation of transparent soil was established, and the pixel intensity was used to characterize the saturation of transparent soil, which could realize the simulation of preferential seepage process of unsaturated transparent soil.

(2) The profile of the full connection preferential flow path (O-O type) and the upper connection preferential flow path (O-C type) presented a T-shape. In the O-O type, most of the fluid directly reached the bottom boundary through the path, and the infiltration rate remained stable. Only part of the soil infiltrated horizontally along the side wall of the path, and the saturation of the profile near the central axis of the path was significantly different from the edge. In the O-C type, the fluid rapidly filled the preferential flow path and diffused to the surrounding soil along the path. With the continuous infiltration, the matrix potential of soil decreased and the infiltration rate tended to be stable. The soil was gradually saturated from the preferential flow path to both sides. In the lower connection preferential flow path (C-O type), the soil oil pressure and matrix potential were not enough to make the pore fluid enter the path to form the preferential flow, which was consistent with the infiltration trend of uniform flow. The stable infiltration rate of the O-C type preferential flow was 1.5 times that of the C-O type preferential flow, and the wetting front moving velocity of the O-C type preferential flow was 1.4 times that of the C-O type preferential flow.

(3) The rotation angle of the adjacent O-C type preferential flow path affected the infiltration path, and a new preferential flow was formed in the area between the preferential flows. The soil first reached a higher saturation, and the growth rate of the saturation decreased with the increase of the rotation angle. At the initial stage of infiltration, the infiltration rate was large, and then it decreased sharply and gradually tended to a flat state. The soil saturation between adjacent preferential flows was higher than that on both sides of preferential flows. With the increase of rotation angle, the infiltration rate and infiltration volume increased correspondingly. The stable infiltration rate of adjacent preferential flow with the rotation angle of 90°, 60°, and 30° was 1.5, 1.3, and 1.2 times that of uniform flow, respectively. Under the action of gravity, the preferential flow with a small rotation angle only infiltrated horizontally along one side of the path. However, the moving depth of the wetting front decreased, and the advancing velocity of the wetting front was 1.3, 1.4, and 1.5 times that of uniform flow, respectively. Due to the weakening of adjacent preferential flow interactions, it was difficult to form a consistent preferential infiltration channel.

References

[1] ALLAIRESUZANNE E, BOCHOVEERIC V, DENAULT J T, et al. Preferential pathways of phosphorus movement from agricultural land to water bodies in the Canadian Great Lakes basin: a predictive tool[J]. Canadian Journal of Soil Science, 2011, 91(3): 361−374.

[2] STONE W W, WILSON J T. Preferential flow estimates to an agricultural tile drain with implications for glyphosate transport[J]. Journal of Environmental Quality, 2006, 35(5): 1825−1835.

[3] LINDAHL A M L, BOCKSTALLER C. An indicator of pesticide leaching risk to groundwater[J]. Ecological Indicators, 2012, 23: 95−108.

[4] JARVIS N J. A review of non-equilibrium water flow and solute transport in soil macropores: principles, controlling factors and consequences for water quality[J]. European Journal of Soil Science, 2007, 58(3): 523−546.

[5] CLOTHIER B E, GREEN S R, DEURER M. Preferential flow and transport in soil: progress and prognosis[J]. European Journal of Soil Science, 2007, 59(1): 2−13.

[6] HENDRICKX J M H, FLURY M. Uniform and preferential flow mechanisms in the vadose zone[C]// Conceptual Models of Flow and Transport in the Fractured Vadose Zone. Washington DC: National Academy Press, 2001: 149−187.

[7] MORRIS C, MOONEY S J. A high-resolution system for the quantification of preferential flow in undisturbed soil using observations of tracers[J]. Geoderma, 2004, 118(1): 133−143.

[8] LI Wen-feng, ZHANG Xiao-ping, LIANG Ai-zhen, et al. Characters of infiltration and preferential flow of black soil in Northeast China under different tillage patterns[J]. Chinese Journal of Applied Ecology, 2008, 19(7): 1506−1510.

[9] WANG K, ZHANG R D. Heterogeneous soil water flow and macropores described with combined tracers of dye and iodine[J]. Journal of Hydrology, 2011, 397(1-2): 105−117.

[10] NI Yu-wen, QU Zi-qing, YING Pei-feng. Preferential flow and its effect on solute migration in soil[J]. Chinese Journal of Applied Ecology, 2001, 12(1): 103−107.

[11] GAZIS C, FENG X H. A stable isotope study of soil water: evidence for mixing and preferential flow paths[J]. Geoderma, 2004, 119(1): 97−111.

[12] MANNHEIMER R, OSWALD C. Development of transparent porous media with permeability and comparable to soils, aquifers, and petroleum reservoirs[J]. Ground Water, 1993, 31(5): 781−788.

[13] ISKANDER M. A transparent material to model the geotechnical properties of soils[C]//Proceedings of ICSMFE. Hamburg, Germany: [s. n.], 1997(1): 315−319.

[14] KONG Gang-qiang, LIU Lu, LIU Han-long, et al. Comparative analysis of the strength characteristics of transparent glass sand and standard sand[J]. Journal of Building Materials, 2014, 17(2): 250−255.

[15] CAO Zhao-hu, KONG Gang-qiang, ZHOU Hang, et al. Model test on installation effect of tapered piles in transparent soils[J]. Rock and Soil Mechanics, 2015, 36(5): 1363−1367, 1374.

[16] ZHOU Hang, YUAN Jing-rong, LIU Han-long, et al. Model test of rectangular pile penetration effect in transparent soil[J]. Rock and Soil Mechanics, 2019, 40(11): 4429−4438.

[17] LENG Xian-lun, WANG Chuan, PANG Rong, et al. Experimental study on the strength characteristics of a transparent cemented soil[J]. Rock and Soil Mechanics, 2021, 42(8): 2059−2068, 2077.

[18] ISKANDER M. Modelling with transparent soils: visualizing soil structure interaction and multi phase flow, Non-intrusively[M]. [S. l.]: Springer, 2010.

[19] LIU J Y. Visualization of 3-D deformations using transparent “soil” models[D]. New York: Polytechnic University, 2003.

[20] TABE K, ISKANDER M, HONMA S. Transparent aquabeads to visualize flow in porous material[J]. Advanced Materials Research, 2011, 239: 2602−2605.

[21] LO H, TABE K, ISKANDER M, et al. Modeling of multi-phase flow and surfactant flushing using transparent aquabeads[C]//Geocongress. [S. l.]: ASCE, 2014.

[22] KASHUK S, MERCURIO S R, ISKANDER M. Visualization of dyed NAPL concentration in transparent porous media using color space components[J]. Journal of Contaminant Hydrology, 2014, 162-163(5): 1−16.

[23] SERRANO R F, ISKANDER M, TABE K. 3D contaminant flow imaging in transparent granular porous media[J]. Geotechnique Letters, 2011, 1(3): 71−78.

[24] PETERS S. Use of transparent soil to model the unsaturated flow characteristics of one-dimensional infiltration with air entrapment[D]. Canada: Royal Military College of Canada, 2011.

[25] LIU Dong-ping, WANG Jin-guo, ZHENG Hu. Advances of soil permeability characteristics based on transparent soil experimental technique[J]. Geotechnical Investigation & Surveying, 2019, 47(1): 1−6, 23.

[26] PETERS S B, SIEMENS G, TAKE W A. Characterization of transparent soil for unsaturated applications[J]. Geotechnical Testing Journal, 2011, 34(5): 445−456.